A standardized method for characterization of matrix effects in laser-induced breakdown spectroscopy

E. Rollin, Olivier Musset, G. Legay, T. Vercouter, J.-B. Sirven

Version of Record: https://www.sciencedirect.com/science/article/pii/S0584854721000896
Manuscript_29665a81d8e67ad4a68bd9468725233d

A standardized method for characterization of matrix effects in laser-induced breakdown spectroscopy

E. Rollin[1], O. Musset[2], G. Legay[3], T. Vercouter[1], J.-B. Sirven[1]*

[1] Université Paris-Saclay, CEA, Service d'Études Analytiques et de Réactivité des Surfaces, F-91191, Gif-sur-Yvette, France

[2] Université Bourgogne Franche Comté, Laboratoire Interdisciplinaire Carnot de Bourgogne, UMR CNRS 6303, F-21078 Dijon, France

[3] CEA, Valduc, F-21120 Is-sur-Tille, France

** corresponding author*

ABSTRACT

The dried droplet method is proposed as a way of characterizing matrix effects in LIBS with a standardized approach. This method was introduced first in the field of LA-ICPMS for quantitative analysis of solids. It consists in depositing a droplet of an iron-containing solution on the sample surface and ablating the dry residue. Then, iron lines are used for spectroscopic diagnoses of the plasma. Along with white-light profilometry analysis for ablation craters measurements, this aims to accurately determine differences of ablated mass, electron temperature and number density, including for pure metals. In this paper, we check that the presence of the dry residue does not influence those three factors. Then, the dried droplet method is applied to 14 pure metals. Results show that the number of ablated atoms varies by a factor of 25, while for the electron temperature the maximum gap between the 14 metals is approximately 2000 K, i.e. a relative variation of ~30%. As for the electron density, it could be estimated for only 6 metals and it varies within the measurement uncertainty between 6 and 8 10^{16} cm^{-3}.

1. INTRODUCTION

Laser-induced breakdown spectroscopy (LIBS) is a well-known technique for fast and direct elemental analysis of materials [1]. It is widely developed for solids both for qualitative measurements, e.g. samples classification, and for quantitative analysis. Since LIBS is based on the interaction between a laser pulse and the sample surface, it is prone to matrix effects stemming from the variation of the sample physical properties. Factors such as the sample hardness [2], thermal properties [3-5], or work function [6], were found to have an influence on the plasma features. As a result, the ablated mass, the plasma electron temperature and number density, depend in a complex way on the surrounding matrix composition and physicochemical state.

Under the assumption of local thermodynamic equilibrium, the LIBS signal can be described by the Boltzmann and Saha-Boltzmann equations involving those three parameters. Therefore, their determination enables both to characterize matrix effects and to correct their influence on the LIBS signal. This approach is the core foundation of the well-known calibration-free method for quantitative analysis by LIBS, which has the great advantage to eliminate the need of external

calibration using matrix-matched samples [7]. Various related methods were proposed since the first paper published in 1999, including recently [8].

Different techniques are implemented to determine the sample ablated mass, the plasma electron temperature and number density. The ablated mass can be measured using white light interferometry [9], optical coherence tomography [10] or X-ray tomography [11]. The plasma parameters are generally determined using a Boltzmann plot for the electron temperature T_e, and the Stark broadening of emission lines for the electron number density n_e. Many other approaches exist but they are less common in LIBS [12].

Let us note that those two widely used methods are based on a selection of suitable lines whose spectroscopic parameters must be known: excitation energy, transition probability, Stark broadening parameter. Consequently, they depend on the sample and on the choice of lines. Obviously, in the extreme case of pure metals, no common set of lines can be used. For multi-elemental samples, it is possible to select lines of a favorable element present in all the samples [13] or from the ambient atmosphere [14]. In any case, whatever the sample composition, several effects such as self-absorption and spectral interferences by lines of matrix, minor or trace elements, are likely to induce a bias on the lines intensity. They can also limit the choice of usable lines to weaker, less repeatable ones, or whose spectroscopic parameters are less accurately known. Then, the resulting uncertainty on T_e and n_e depends on the matrix and from a fundamental point of view, the question can be raised whether the plasma electron temperature and number density, as measured with different lines from one material to the other, are comparable.

The objective of this paper is to accurately characterize matrix effects observed in plasmas produced by laser ablation of 14 pure metals, in terms of ablated mass, electron temperature and number density. The first one was measured by optical profilometry. For the determination of plasma parameters, our approach consisted in depositing a droplet of an iron-containing solution on the metal surface and ablating the dry residue [15,16]. The choice of iron lines used was then carefully optimized to minimize possible biases in the determination of T_e and n_e by the Boltzmann plot and Stark broadening methods. Results show that the number of ablated atoms varies by a factor of 25 over the 14 metals, whereas the actual difference of electron temperature does not exceed 2000 K. As for the electron number density, it ranges from 6 to 8 10^{16} cm^{-3} in our experimental conditions.

2. MATERIALS AND METHODS

2.1. Samples

The electron temperature was determined both by a standard approach and by the dried droplet method using aluminum, copper, nickel and titanium alloys containing iron. Their composition is given in Table 1.

Table 1 Composition of alloys used in this study, in mass %.

Matrix:	Aluminum								Copper				Nickel			Titanium		
Reference	51XG00H2	637C/01	311/01	124/04	35831	63698	198F	52963	CT1	CT2	CT3	CT5	B7011	B7004	F294	IA271A	BST22	BSTSU-1

Al	98.4	95.2	98.5	99.1	97.5	95.1	99.99	98.7	-	-	-	-	1.2	1.64	0.05	5.28	0.004	6.11
Cu	0.111	0.379	0.044	0.053	0.065	0.4	0.005	0.02	97.8	98.4	99	98.4	0.07	0.14	0.11	0.004	0.04	0.073
Fe	0.356	0.377	0.21	0.145	0.558	0.81	0.001	0.11	0.17	0.1	0.083	0.016	0.34	0.97	0.06	0.31	1.19	0.22
Ni	0.119	0.103	0.05	0.059	0.058	-	-	-	0.48	0.29	0.12	0.01	58.2	74.6	99	0.035	0.008	0.073
Ti	0.128	0.065	0.09	0.051	0.166	0.06	-	0.06	-	-	-	-	2.05	2.63	0.03	91.5	93.2	88.2

Then, the dried droplet method was applied to 14 metals: Al, Cr, Cu, Mn, Mo, Ni, Si, Sn, Ta, Ti, W, Y, Zn, Zr. The 14 metals purity was higher than 99.9% except for Cr (99.8%) and Ti (99.4%).

2.2. The dried droplet method

The dried droplet method was implemented by Villasenor et al. in LA-ICP-MS as a way to perform standard addition on solid materials for quantitation of impurities [15,16]. Here, we use it in order to introduce a suitable tracer element for plasma characterization, in a plasma formed on a matrix that does not contain this element. Since it is widely studied for spectroscopic diagnoses of laser ablation plasmas, we chose iron [17]. Then, the method principle is to deposit on the sample surface a 5-µL droplet of an iron solution. The droplet is manually spread, using the tip of the pipette, over an approximately 15x5 mm rectangular surface, then samples are dried in ambient air inside a fume cupboard. The dry residue is finally ablated with the substrate and iron lines are detected.

We used an iron chloride solution ($FeCl_3$, Emsure, purity higher than 99%) with w = 10 % Fe. It was successively diluted to make 10-ppm, 20-ppm and 100-ppm solutions. The deposit thickness was characterized by GD-OES (Horiba GD-Profiler 2). For a 20-ppm droplet on pure copper, Figure 1 shows that the deposit thickness is of the order of 20 nm.

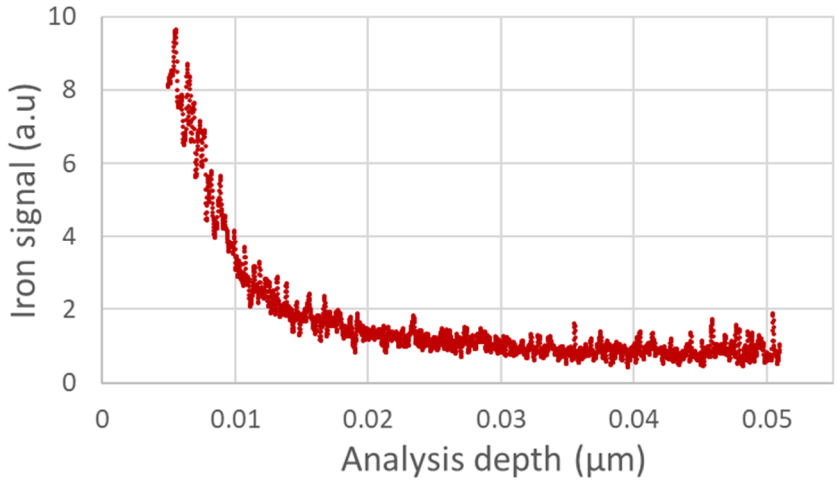

Figure 1 Glow discharge – optical emission spectroscopy analysis of a 20-ppm iron chloride deposit on the surface of a copper sample.

2.3. Experimental setup and measuring protocol

A commercial LIBS system was used for the measurements (Mobilibs, IVEA). It included a 266 nm YAG laser delivering 4 ns pulses (full width at half-maximum) with an energy of 7 mJ at a 20 Hz repetition rate. The laser spot diameter on the sample surface was 50 µm. The optical system for plasma light collection imaged the plasma with a 1/4 magnification at the entrance of a 910 µm

optical fiber. Thus, the plasma emission was spatially integrated. We used a 1 m monochromator equipped with a 2400 grooves/mm grating (Horiba THR1000) and with an intensified CCD with 2048x512 pixels of 13.5 µm (Andor iStar). Spectra were recorded between 371.7 and 380.5 nm in a single acquisition, with a linear dispersion of 4.65 pm/pixel. The instrumental Gaussian width was measured using a hollow cathode lamp and was found equal to 22.9 pm in this spectral range.

For measurements on aluminum, copper, nickel and titanium alloys, 20 laser shots were accumulated at each sample location and 200 spectra were recorded. They were subsequently averaged by groups of 20, leading to 10 replicas of 400 laser shots each. The detection gate delay was 1 µs and the LIBS signal was integrated over 9 µs. Obviously plasma parameters change within this temporal window. Yet, the reason of this choice was that due to different physical properties (particularly thermal and chemical ones), the temporal dynamics of the plasma can vary significantly from one sample to the other. Then, to compare different materials, the electron temperature within a given time gate was considered less meaningful than the average temperature over the whole plasma emission lifetime, which we took equal to 10 µs. Although there is no local thermodynamic equilibrium (LTE) over such a long duration, this enabled to compensate for different temporal dynamics from one matrix to the other. In these experimental conditions, we checked that the McWhirter criterion was satisfied, that the linearity of Boltzmann plots was equivalent to that obtained with a 500-ns gate width, and that the temperature obtained from Fe or Ti lines was identical (this last point could be checked only for aluminum alloys). This shows that the lines levels used for spectroscopic measurements could reasonably be considered as close to the Boltzmann equilibrium, even if LTE was not strictly satisfied.

For measurements based on the dried droplet method, the gate delay was 1 µs and the gate width was 0.5 µs. In our irradiance conditions (90 GW/cm² for a 7 mJ pulse), the ablation depth per laser shot was found higher than 1 µm for all samples. Consequently, most of the iron signal stemming from the 20-nm deposit was obtained in a single laser shot and we chose to move the sample during the acquisition at 3 mm/s. Several hundreds of single-shot spectra were recorded over the residue surface with 150 µm between successive shots. Due to the irregular shape of the deposit, a fraction of laser shots ablated the naked surface. Spectra with and without deposit were sorted based on the Fe 373.49 nm line intensity. Spectra were rejected if this intensity was lower than that of the naked sample plus two standard deviations. Spectra recorded on the deposit were subsequently averaged by groups of 200. Finally, 500 single-shot spectra were also recorded on the sample naked surface in order to measure the average spectrum of the pure sample for background correction.

The volume of ablation craters was measured by a white light optical profilometer (Bruker Contour GT1). When the crater exhibited a rim above the sample surface, its volume was subtracted to that of the crater below the surface. This mainly happened with aluminum samples and when several laser shots were accumulated at a given sample location.

The electron temperature was measured by the Boltzmann plot method based on neutral iron lines. The electron number density was determined from the Stark broadening of some of those lines. This broadening was relatively weak: the full width at half-maximum of iron lines $\Delta\lambda_{TOT}$ was typically between 25 and 28 pm, while the instrumental width $\Delta\lambda_{instrumental}$ was 22.9 pm. Therefore, the line profile was more accurately fit by a Gaussian profile than by a Voigt one. The Stark width $\Delta\lambda_{Stark}$ was then calculated using the following expression taken from ref. [18]:

$$\Delta\lambda_{TOT} = 0.5346\ \Delta\lambda_{Stark} + (0.2169\ \Delta\lambda^2_{Stark} + \Delta\lambda^2_{Gauss})^{1/2}$$

With $\Delta\lambda^2_{Gauss} = \Delta\lambda^2_{instrumental} + \Delta\lambda^2_{Doppler} = \Delta\lambda^2_{instrumental} + [\lambda_0 \times 7.16\ 10^{-7} \times \sqrt{T/M}\ ]^2$ [12].

Where $\Delta\lambda_{Gauss}$ includes the contributions of the instrumental and Doppler broadening, λ_0 is the line wavelength, T is the plasma temperature (K) and M is the atomic mass (g/mol). The Doppler broadening was of the order of 3 pm and its contribution was in fact negligible compared to the instrumental width. Finally, the electron number density n_e was determined from the simplified expression:

$$n_e = n_e^{ref} \frac{\Delta\lambda_{Stark}}{\Delta\lambda_{Stark}^{ref}}$$

Where $\Delta\lambda_{Stark}^{ref}$ = 9 ± 2 pm for n_e^{ref} = 10^{17} cm^{-3} for the Fe 373.49 nm line [19]. The experimental uncertainty on the Stark width measurement was estimated at 1 pm. Combined with the uncertainty on the Stark broadening coefficient, the global uncertainty on the electron density was about 2.5 10^{16} cm^{-3}.

3. RESULTS AND DISCUSSION

3.1. Determination of the electron temperature from lines of a common element

In view of determining the electron temperature for different materials with a method as close as possible from one sample to the other, a natural idea is to use a common set of lines of a common element. In this section, we discuss this approach on 4 matrices containing iron as an impurity: aluminum, copper, nickel and titanium. All samples of Table 1 were used except for samples 198F, 52963 and CT5 whose iron concentration was too low, i.e. 15 samples in total. In each case, the iron lines were selected if they were free from spectral interference by another line, and if their background-corrected intensity was higher than 3 standard deviations of the background level σ_B. Based on those two criteria, Table 2 shows the selected lines. The electron temperature was first determined from those lines, but for the sake of standardization of the method, we reduced the selection to the five lines common to each matrix, at 371.99, 373.49, 374.95, 376.55 and 376.72 nm. Figure 2a shows the Boltzmann plots obtained in this case, for one sample of each matrix. For those four samples, the experimental repeatability of the temperature measurement was determined from the 10 replicas, and we assumed that it was representative of the repeatability of all samples of a given matrix (Figure 2b). Note that the temperatures found from the complete sets of lines and from the five common ones were identical within this experimental repeatability. Figure 2b shows the temperature obtained for all samples from the spectrum averaged over the 10 replicas, with the average and standard deviation for each matrix.

Table 2 Iron lines selected for each matrix for electron temperature measurement by the Boltzmann plot method: wavelength (λ, nm), lower level energy (E_j, eV), upper level energy (E_i, eV), upper level statistical weight (g), transition probability (A, 10^8 s^{-1}).

λ	E_j	E_i	gA	Fe lines selection for each matrix			
nm	eV	eV	10^8 s^{-1}	Al	Cu	Ni	Ti
371.99	0	3.33	1.782	✓	✓	✓	✓
372.26	0.09	3.42	0.249	✖	✓	✖	✖
372.76	0.96	4.28	1.12	✓	✓	✓	✖
373.24	2.2	5.52	1.345	✓	✖	✖	✖

373.35	0.11	3.43	0.194	✓	✗	✗	✗
373.49	0.86	4.18	9.911	✓	✓	✓	✓
373.71	0.05	3.37	1.269	✓	✓	✗	✗
374.83	0.11	3.42	0.458	✓	✓	✗	✗
374.95	0.92	4.22	6.867	✓	✓	✓	✓
375.82	0.96	4.26	4.438	✓	✓	✗	✗
376.38	0.99	4.28	2.72	✓	✓	✓	✗
376.55	3.24	6.53	14.265	✓	✓	✓	✓
376.72	1.01	4.3	1.917	✓	✓	✓	✓
378.79	1.01	4.28	0.645	✓	✓	✓	✗
379.50	0.99	4.26	0.805	✗	✓	✗	✗

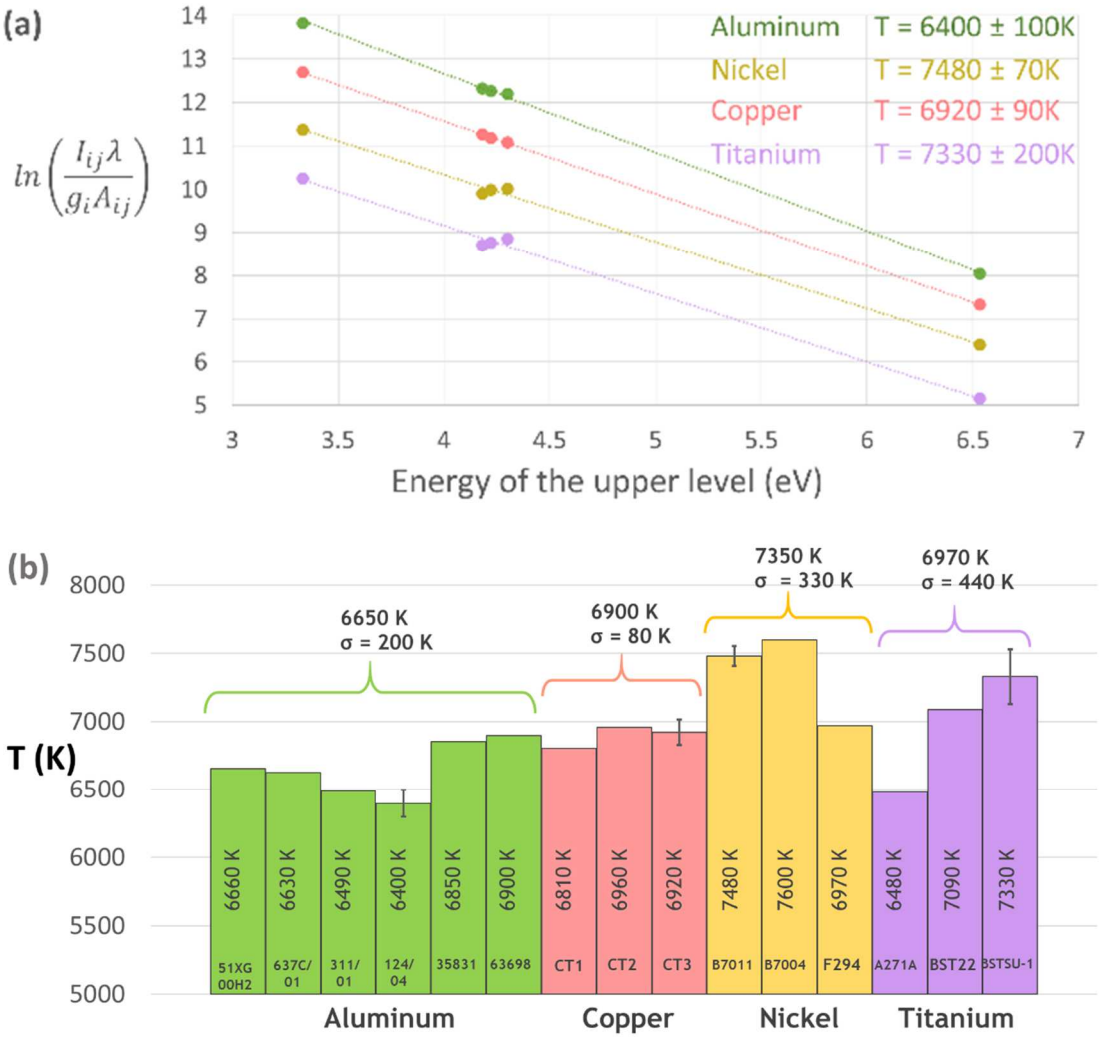

Figure 2 (a) Boltzmann plots obtained for one sample of each matrix using a common set of 5 iron lines; (b) Electron temperature obtained for all samples.

We get an average temperature different for each matrix, which shows the presence of a matrix effect, although limited. Indeed, the intra-matrix dispersion is relatively high compared to the

temperature gap between matrices. In the case of aluminum, nickel and titanium, we note that this dispersion is significantly higher than the experimental repeatability for the samples in which this repeatability has been extensively evaluated (Figure 2a). However, we would have expected that different samples of a same matrix would lead to a common value of plasma temperature, assuming that the plasma temperature is dependent on the matrix rather than on the minor or trace elements. Then, these results tend to indicate that the intra-matrix uncertainty may be affected by a systematic error. As the set of lines used for the Boltzmann plot is the same for all samples, the choice of lines plays no role. As they were selected if they were free from spectral interference, this phenomenon is not in question either. In contrast, self-absorption is likely to induce a bias on the line intensity. The element concentration in the plasma is an important factor of self-absorption. To investigate this effect, Figure 3 shows the electron temperature measured for the six aluminum alloys as a function of the iron concentration. We observe a clear correlation: the apparent temperature is all the higher as the iron concentration is high. This can be attributed to the under-estimation of the intensity of lines with a high transition probability and/or a lower level of low energy, leading to an over-estimation of the electron temperature. This is particularly the case of the 371.99 nm line with the lowest excitation energy in the Boltzmann plot, but we cannot exclude that the three lines with an upper level energy around 4.2 eV are subject to self-absorption as well, though to a lesser extent.

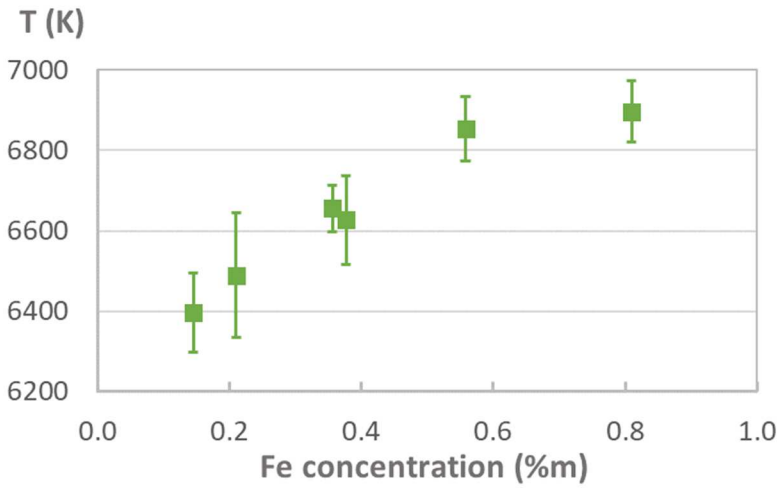

Figure 3 Apparent electron temperature as a function of the iron concentration in the sample, for the 6 aluminum alloys measured on Figure 2.

Finally, the determination of the electron temperature in plasmas formed on different metal matrices using a common set of iron lines does not enable to characterize matrix effects with a sufficient accuracy, since the measurement is variably affected by self-absorption of low energy lines. With our reduced set of five lines, removing the ones suspected of self-absorption is not a robust option. Moreover, this approach cannot be restricted to samples with the same (low) iron concentration. This is simply not applicable. Eventually, this approach is of course not feasible with pure metals. Therefore, we propose an alternative in the next section.

3.2. Determination of the electron temperature and number density by the dried droplet method

3.2.1. Method optimization and validation

The dried droplet method was implemented in order to characterize the ablated mass, the electron temperature and number density with a standardized method, applicable to any pure material. For the method to be valid, the presence of the deposit on the sample surface must not significantly affect those three parameters, and spectroscopic determination of plasma features must not be biased. For that purpose, two factors can be optimized: the concentration of the iron solution deposited on the sample surface, and the selection of iron lines in order to eliminate, or at least minimize, possible self-absorption effects. This was investigated using standard samples of aluminum and copper alloys containing iron, thus enabling to determine the plasma parameters with and without deposit with the same iron lines. Samples 51XG00H2, 52963 and 198F were used for aluminum, while samples CT1, CT3 and CT5 were used for copper (see Table 1).

Figure 4 shows the volume of the ablation crater produced by a single laser shot in the least concentrated samples, the aluminum alloy 198F containing 10 ppm of iron, and the copper alloy CT5 containing 160 ppm of iron. The measurement was performed on the naked surface and on the sample with a residue of a 10-ppm and 100-ppm iron solution. Error bars represent one standard deviation over 5 craters. Note that with a 20-nm thick deposit, its volume over the laser spot surface is lower than 100 μm^3, negligible compared to the crater volume. For aluminum, there seems to be a trend on the ablated volume with the deposit concentration, which would indicate that the presence of the deposit modifies the sample absorption efficiency and the crater volume. Yet, the three measurements remain within one standard deviation. In addition, as shown below, a 10-ppm solution was found sufficient to implement the dried droplet method, hence minimizing this effect if it exists. For copper, we detected no influence of the deposit on the ablated volume. Note that Villasenor et al. concluded the same in their experimental conditions with alumina-based samples [15].

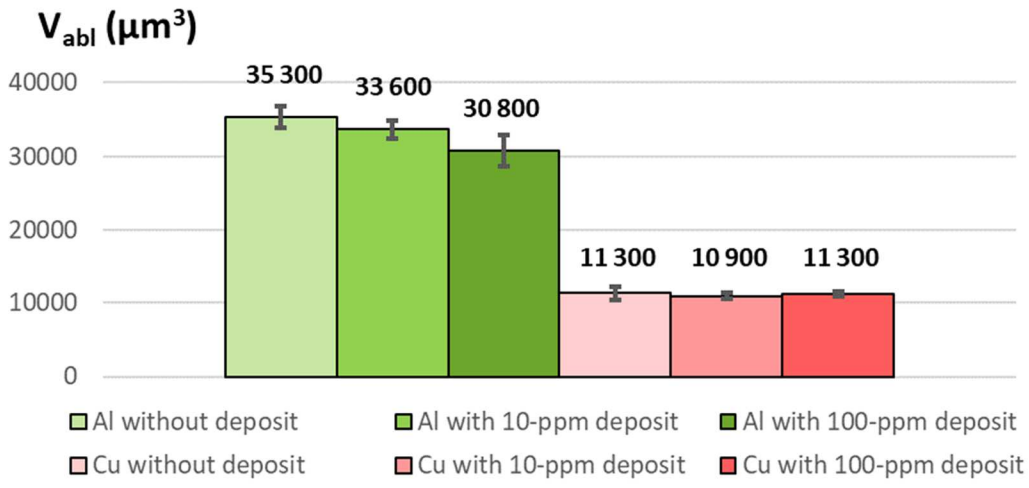

Figure 4 Average ablated volume obtained for the 198F aluminum sample (10 ppm Fe) and for the CT5 copper sample (160 ppm Fe), without any deposit, and with a 10-ppm and 100-ppm iron chloride residue on the surface.

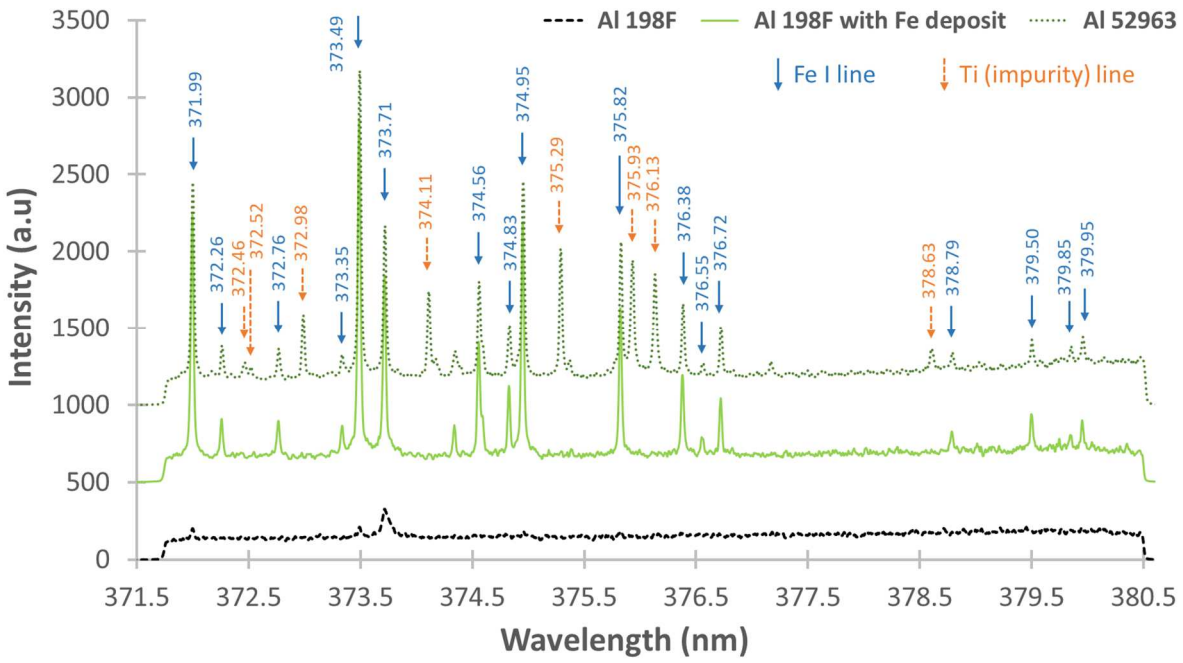

Figure 5 LIBS spectra of three aluminum samples: a quasi-pure one (198F, 10 ppm of iron), an alloy containing 0.11% of iron (52963), and the 198F sample with a 10-ppm solution deposit. Iron and titanium lines are indicated by arrows. Spectra are vertically shifted for better clarity.

Figure 5 shows the spectra of three aluminum-based samples: an almost pure one (198F, 10 ppm of iron) for which iron lines are not detected, sample 52963 containing 0.11% of iron, for which iron lines are clearly visible, and sample 198F with a 10-ppm solution deposit. We see that this low concentrated deposit enables to introduce iron lines with an intensity equivalent to that of the 52963 sample.

Table 3 Iron lines selected for Boltzmann plots obtained by the dried droplet method, for each matrix: wavelength (λ, nm), lower level energy (E_j, eV), upper level energy (E_i, eV), upper level statistical weight (g), transition probability (A, 10^8 s^{-1}).

Line	λ	E_j	E_i	gA	Method validation on Al and Cu alloys		Fe lines selection for pure metals												
#	nm	eV	eV	10^8 s^{-1}	Initial set of lines	Reduced set of lines	Al	Si	Cu	Zn	Ta	Sn	Ni	Mn	W	Cr	Ti	Zr	Mo	Y
1	371.99	0	3.33	1.782	✓	✘	✘	✘	✘	✘	✘	✘	✘	✘	✘	✘	✓	✓	✘	✘
2	372.26	0.09	3.42	0.249	✓	✓	✓	✓	✓	✓	✓	✓	✘	✓	✓	✓	✘	✓	✓	✓
3	372.76	0.96	4.28	1.12	✓	✓	✓	✓	✓	✓	✓	✓	✓	✓	✓	✓	✓	✘	✘	✓
4	373.24	2.2	5.52	1.345	✓	✓	✓	✓	✓	✓	✓	✓	✓	✘	✘	✘	✓	✘	✘	✘
5	373.35	0.11	3.43	0.194	✓	✓	✓	✓	✓	✓	✓	✓	✓	✓	✓	✓	✓	✓	✓	✓
6	373.49	0.86	4.18	9.911	✓	✘	✘	✘	✘	✘	✘	✘	✘	✘	✘	✘	✘	✓	✘	✘
7	373.71	0.05	3.37	1.269	✓	✘	✘	✘	✘	✘	✘	✘	✘	✘	✘	✘	✘	✓	✘	✘
8	374.83	0.11	3.42	0.458	✓	✓	✓	✓	✓	✓	✓	✓	✓	✓	✓	✓	✘	✓	✓	✘
9	374.95	0.92	4.22	6.867	✓	✘	✘	✘	✘	✘	✘	✘	✘	✘	✘	✘	✘	✓	✘	✘
10	375.82	0.96	4.26	4.438	✓	✘	✘	✘	✘	✘	✘	✘	✘	✘	✘	✘	✘	✓	✘	✘

11	376.38	0.99	4.28	2.72	✓	✖	✖	✖	✖	✖	✖	✖	✖	✖	✖	✖	✓	✓	✓	✖
12	376.55	3.24	6.53	14.265	✓	✓	✓	✓	✓	✓	✓	✓	✓	✓	✓	✓	✖	✓	✓	✖
13	376.72	1.01	4.3	1.917	✓	✖	✖	✖	✖	✖	✖	✖	✖	✖	✖	✖	✖	✖	✓	✓
14	378.79	1.01	4.28	0.645	✓	✓	✓	✓	✓	✓	✓	✓	✓	✓	✓	✓	✓	✖	✓	✖
15	379.50	0.99	4.26	0.805	✓	✓	✓	✓	✓	✓	✓	✓	✓	✓	✓	✓	✓	✓	✓	✖
16	379.75	3.237	6.50	5.941	✖	✖	✓	✓	✓	✓	✓	✖	✓	✓	✓	✖	✖	✖	✖	✖
17	379.85	0.915	4.18	0.355	✖	✖	✓	✓	✓	✓	✓	✖	✓	✓	✖	✓	✖	✓	✖	✖
18	379.95	0.958	4.22	0.658	✖	✖	✓	✓	✓	✓	✓	✖	✓	✓	✓	✓	✓	✓	✖	✓

For the electron temperature measurement, all iron lines previously selected for alloys samples (see Table 2) were initially taken into account to trace the Boltzmann plots. Indeed, no spectral interference was detected with these more pure metal samples. Figure 6a shows the Boltzmann plots obtained for the aluminum 52963 sample containing 0.11% of iron, without deposit, and with a 10-, 20- and 100-ppm iron solution deposit. The uncertainty is calculated here from the uncertainty propagation expression given in [17]:

$$\frac{\Delta T_e}{T_e} = \frac{k_B T_e}{E_{i,max} - E_{i,min}} \left(\frac{\Delta I_{ij}}{I_{ij}} + \frac{\Delta A_{ij}}{A_{ij}} \right) \qquad \textit{Equation 1}$$

This expression is originally used when one calculates the electron temperature from the relative intensity of two lines. However, we used it here in the case of a Boltzmann-plot. Since a Boltzmann plot uses multiple lines instead of two, this expression leads us to the "worst-case scenario" of the uncertainty. We considered an uncertainty of 10 % for the lines intensities and of 7 % for the transition probabilities, the highest value among the lines we used, and an energy gap of 6.53-3.33 = 3.20 eV. Using these values, for an electron temperature of 7500 K, we found an uncertainty of 260 K, higher than the experimental repeatability, which is about 100 K. Even though we keep this upper value, we see that the temperature gap between samples with a growing deposit concentration is significant. This would indicate that the presence of a concentrated iron solution residue tends to increase the plasma temperature. Yet, as shown on Figure 6a, some iron lines appear below the regression line. This observation is all the more pronounced for the most intense ones, and for a highly concentrated deposit. This suggests again that self-absorption may induce an under-estimation of those lines intensity, hence an over-estimation of the temperature. As shown by Figure 9a (Supporting information), the temperature increase is correlated to the decrease of the correlation coefficient of the linear regression R^2 by emission lines biased by self-absorption. This degradation is also correlated to the total iron concentration in the plasma, and not only to the deposit concentration, as shown on Figure 9b where the Boltzmann plot intercept is taken as an indicator of this global concentration. Finally, another indicator of self-absorption was measured. In the case of the Al 52963 sample with a 100-ppm deposit, we observed a linear behavior between the iron lines width and their intensity. Such a resonant broadening was not observed for a 10-ppm deposit (Supporting Information, Figure 10).

Therefore, in order to mitigate the issue of self-absorption, emission lines and spectra were selected as follows. Firstly, for each group of lines with an excitation energy around 3.4 and 4.2 eV, we kept only the three ones with the lowest gA, respectively lower than ~0.5 10^8 s^{-1} and ~1.2 10^8 s^{-1}. Hence, only 8 lines remained in total (Table 3). Secondly, given the deposit heterogeneity, we excluded the most intense single-shot spectra, assuming that the risk of self-absorption was higher in the highly concentrated regions of the deposit. The criterion was to eliminate all spectra with an intensity of the

373.49 nm line higher than the average plus one standard deviation. This lead to the exclusion of about 15% of spectra. The Boltzmann plots obtained after this selection of lines and spectra are shown on Figure 6b. Now we see that the electron temperature determined with or without deposit is identical within the measurement uncertainty. We also note that for the naked sample, we obtain the same value as previously, meaning that the lines and spectra selection introduced no additional bias in the temperature determination. For the most concentrated deposits, it also means that without this careful approach, the bias on the temperature can reach several hundreds of Kelvins. As shown by Figure 9, no trend is detectable between the temperature, the correlation coefficient of the linear regression, and the Boltzmann plot intercept. The R^2 is higher than 0.995 in all cases, showing a very good quality of the Boltzmann plot over the range of excitation energy studied here. Finally, provided a suitable selection of lines and spectra to reduce self-absorption effects, this demonstrates that the deposit has no significant effect on the plasma electron temperature.

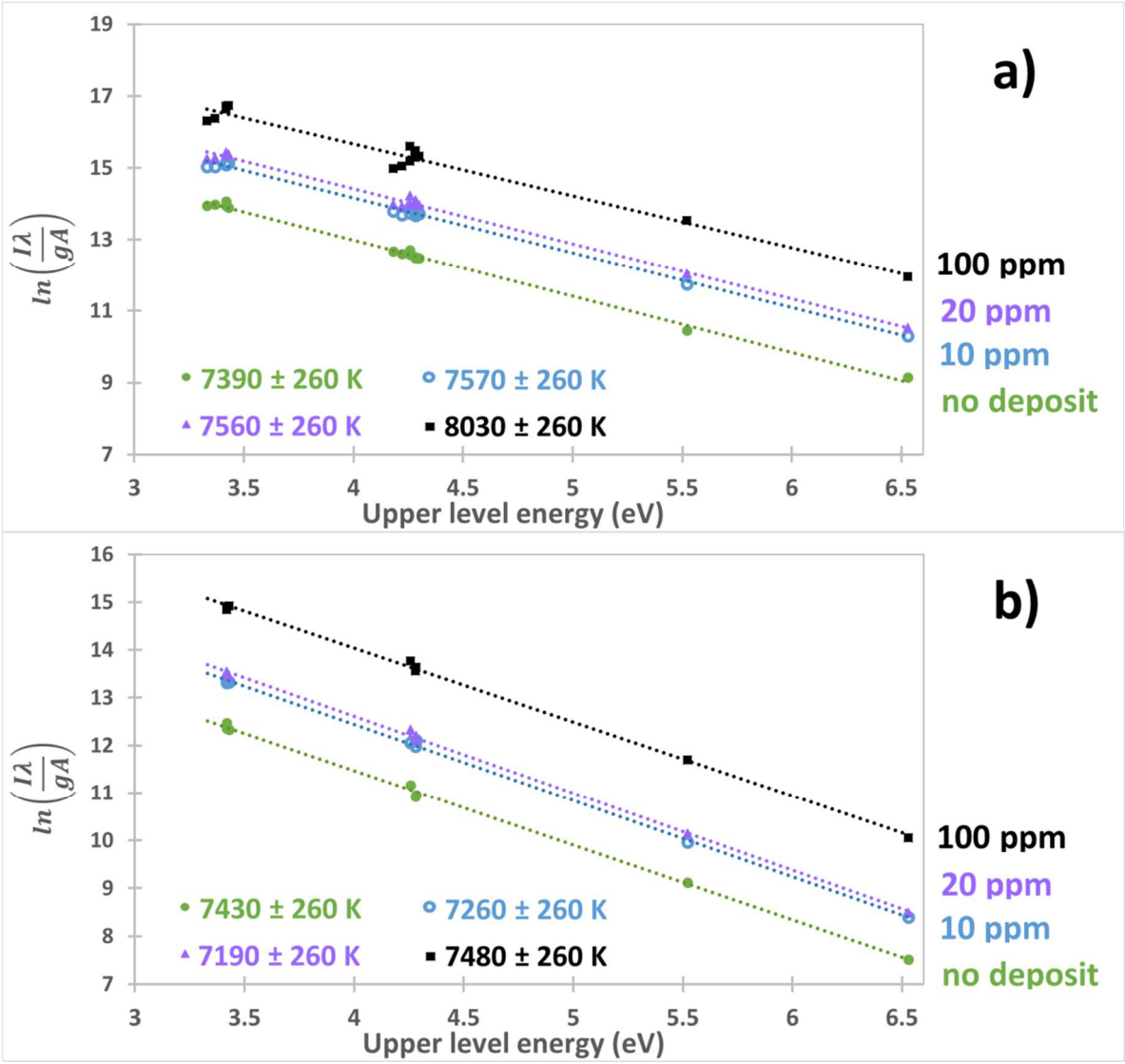

Figure 6 Boltzmann plots obtained for the aluminum 52963 sample, with and without an iron deposit, (a) from the complete set of iron lines (Table 3a), (b) from the reduced set of iron lines (Table 3b).

The electron number density was determined from the set of selected spectra, using the Stark broadening of the 8 iron lines, except for the 373.24 and 373.35 nm ones. The 373.24 nm line was found too weak to determine accurately the Stark width, while the fitting of the 373.35 nm line profile was made difficult by the wing of the intense nearby line at 373.49 nm. The Stark broadening parameter for the 6 lines was taken as 9 ± 2 pm at an electron number density of 10^{17} cm^{-3}. This value can be found in ref. [19] only for the 376.55 nm and 378.79 nm lines. As the 6 lines have a very similar width, we hypothesized that the Stark broadening parameter was the same for all. The Al samples 52963 and 51XG00H2, whose iron concentration is enough to measure the iron lines of interest, were used to determine the density without deposit. For copper, the three samples could be used. Next, the density obtained with the deposit was measured for the three samples of each matrix and the three deposit concentrations. As mentioned in section 2.3, the uncertainty on the electron number density was estimated at 2.5 10^{16} cm^{-3}.

The same approach was implemented for the electron temperature. Results are shown on Figure 7. They illustrate that for both matrices, the plasma parameters are not significantly different with or without the deposit. With the previous measurements of the ablated volume, this completes the validation of the dried droplet method: the presence of the deposit with a concentration up to 100 ppm, does not affect the laser ablation efficiency nor the electron temperature and number density. Therefore, this method can be used to introduce a tracer element suitable for plasma characterization, such as iron, in order to accurately diagnose matrix effects with a standardized approach whatever the material. In particular, it is applicable to pure materials whose emission lines are not always favorable for spectroscopic measurements. Eventually, it avoids a systematic and fastidious work to select, for each material under study, suitable lines for spectroscopic diagnoses of the plasma.

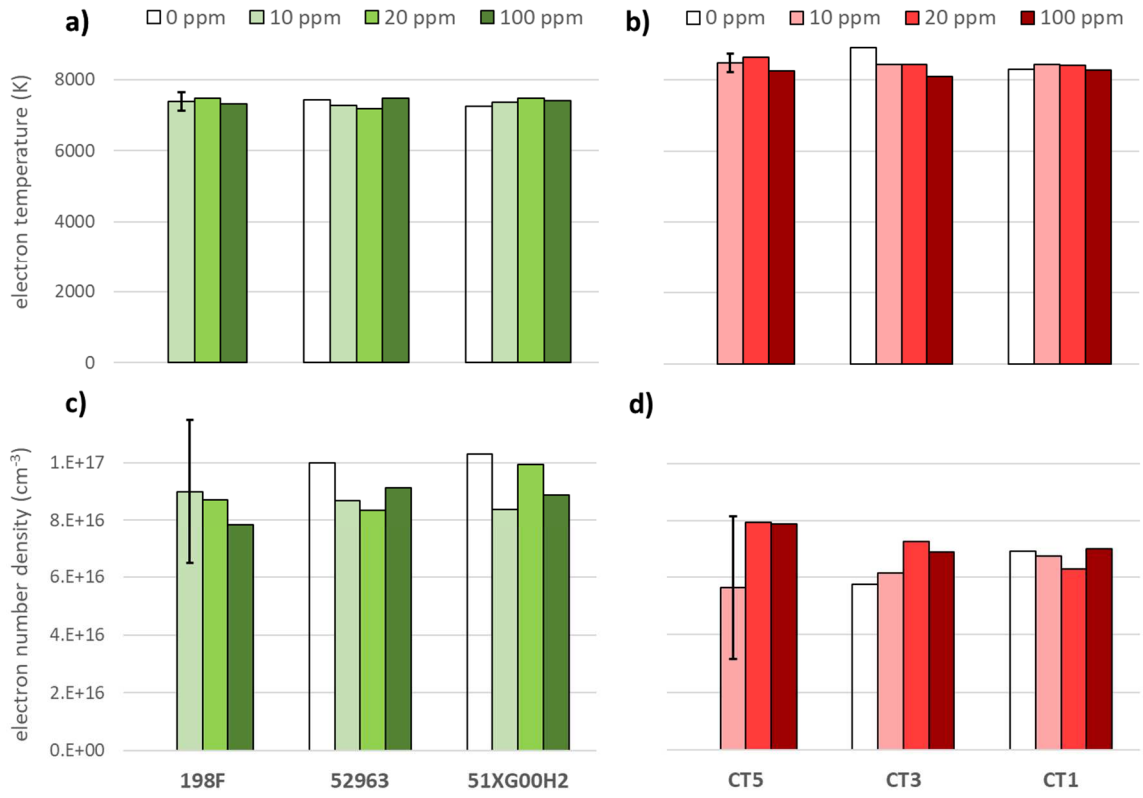

Figure 7 Electron temperature (a and b) and number density (c and d) measured by the dried droplet method for three aluminum (a and c) and three copper (b and d) samples. Each sample was measured without any deposit and with a 10-, 20- and 100-ppm iron chloride deposit. For low-concentrated samples 198F and CT5, without deposit the iron signal was too low

to properly measure the temperature and density. Error bars are equal to 260 K for the electron temperature and 2.5 10^{16} cm^{-3} for the electron number density.

3.2.2. Characterization of matrix effects for pure metals

The dried droplet method was applied to 14 quasi-pure metals to characterize matrix effects. A 40-ppm iron chloride solution was deposited on the samples surface, and samples were dried on a hot plate at 80°C. The laser pulse energy was 5 mJ. Other experimental conditions were the same as those described in the Experimental section. Single-shot ablation craters were measured by optical profilometry, and the electron temperature and number density were determined using the dried droplet method presented in the previous section, with two differences. Firstly, the iron lines spectrum was obtained by subtracting the sample spectra with and without deposit. Figure 11 (Supporting Information) illustrates that in the case of titanium, and shows that the reproducibility of matrix lines with and without deposit is very good, thus enabling to clearly highlight iron ones in the background-corrected spectrum. Secondly, due to variable spectral interferences with the matrix element, the lines selection had to be adjusted for each metal. We used the following rules to select lines of interest:

1. Absence of spectral interference by a matrix line.
2. There should be at least three groups of excitation energy among the four ones available: ~3.4 eV (5 lines), ~4.2 eV (10 lines), 5.5 eV (1 line) and ~6.5 eV (2 lines). Only yttrium did not fulfill this condition.
3. The 7 most intense lines, most likely to be self-absorbed, were excluded: lines at 371.99, 373.49, 373.71, 374.95, 375.82, 376.38 and 376.72 nm.
4. For Ti, Zr, Mo and Y giving the most line-dense spectra, one or several lines among this list of 7 were selected anyway in order to ensure a sufficient redundancy for both groups of lines around 3.4 and 4.2 eV.

For each metal, Table 3 shows the lines selected to trace the Boltzmann plot, and Figure 8 shows the results for the ablated mass and the electron temperature. Note that due to a poor surface state and to a very low ablation efficiency, ablation craters could not be observed for manganese, even though a LIBS signal could be detected. We see that the ablated mass varies by a factor of more than 5 over the 13 remaining metals. Taking into account the atomic weight of each element, this is equivalent to a factor of 25 in terms of number of ablated atoms. Therefore, there is a significant matrix effect regarding the laser ablation of metals, which was already observed in several publications [4,13,20,21]. Concerning the electron temperature, the maximum gap between the 14 metals is approximately 2000 K, between Mo and Ni, i.e. a relative increase of ~30%.

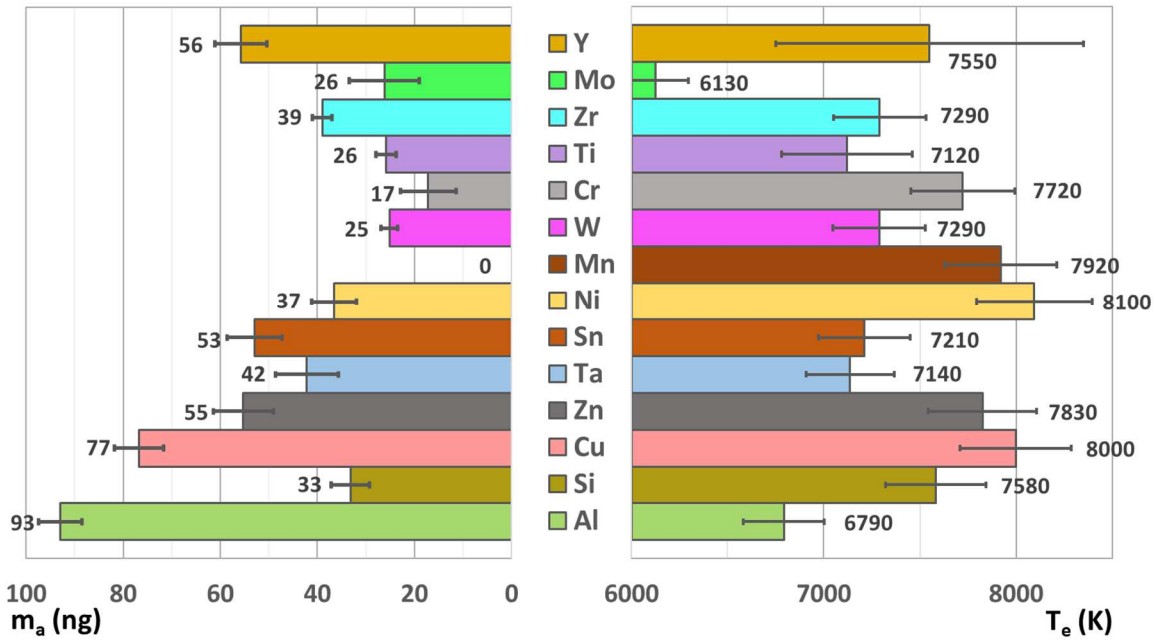

Figure 8 Ablated mass and electron temperature measured on 14 pure metals by the dried droplet method. For the ablated mass, error bars are 1 standard deviation over 5 craters. For the temperature, they are calculated from Equation 1.

As for the electron number density, it was possible to measure it in all metals from the Stark broadening of the 373.49 nm line. However, we found that this intense line was self-absorbed in many cases, leading to an over-estimation of the density due to resonant broadening. Therefore, we selected a set of weak lines (number 2, 3, 5, 8, 14 and 15 in Table 3), but then the density could be measured only in Al, Si, Cu, Zn, Ta and Sn. The average Stark broadening of those 6 lines was calculated. We obtained an electron number density of 8 10^{16} cm^{-3} for Al and 6 10^{16} cm^{-3} for other metals, with a measurement uncertainty of the order of 2.5 10^{16} cm^{-3}. Therefore, for those 6 metals, the electron density varied within the measurement uncertainty, while the number of ablated atoms varied by a factor of 15 and the electron temperature by ~18%.

3.2.3. Discussion

The objective of this paper was to determine as accurately as possible the extent of matrix effects observed in LIBS plasmas produced on 14 pure metals. Those effects are revealed by differences in ablated mass, plasma electron temperature and number density. The ablated mass showed differences from one metal to the other up to a factor of 25 in terms of number of ablated atoms. This gap is very significant, yet one should remember that the craters measurement by white-light profilometry only gives the amount of displaced matter. It does not take into account the atomization yield, which drives the number of atoms in vapor phase that feed the plasma. A more accurate diagnosis of the ablation efficiency would be to determine the absolute number of atoms in the plasma, for instance by calibrating the detection system in number of photons.

The electron temperature was measured by the most widespread method in LIBS, namely the Boltzmann plot method. With pure samples, obviously it is impossible to implement this approach from the same spectral lines. In principle, it is possible to use lines of each pure matrix, but there are a few obstacles. Finding emission lines that are not interfered, nor self-absorbed, with known

spectroscopic parameters, intense enough and within a sufficiently large range of excitation energy, is a tedious work. The alternative consisting in measuring lines of a common minor or trace element was found limited by its uncontrolled concentration over the samples set, leading to a variable degree of self-absorption. In addition, as shown in this paper, the choice of emission lines must be carefully studied to avoid any bias on the temperature, an over-estimation that can reach several hundreds of Kelvins. This is significant, since it is of the same order of magnitude as the temperature difference observed between most metals. It is also significant from an analytical point of view, e.g. for calibration-free purposes. Indeed, from the Boltzmann and Saha equations, in a plasma with an electron number density of 10^{17} cm^{-3}, the intensity of the Fe I line at 404.58 nm increases by 34% when the electron temperature raises by 7%, from 7000 to 7500 K.

The dried droplet method is an attempt to standardize the determination of the electron temperature so that the obtained values are more comparable from one material to the other. By introducing in the plasma a tracer element in the form of a surface deposit, the same element and the same initial set of emission lines can be used whatever the material. This initial set still needs to be adjusted, mainly due to spectral interferences that vary from matrix to matrix. This can be delicate for spectroscopically dense materials, although the background correction by the spectra of the sample without deposit is easy and very helpful to highlight the tracer emission lines. In any case, the methodology remains the same for all metals and possible biases on the electron temperature are limited.

The determination of the electron number density by the Stark broadening of selected lines was more tricky. The most favorable lines for such a measurement, those whose broadening parameter is high, have a high excitation energy. Thus, they are more suited to major elements, but not to low concentrated ones such as the tracer element used in the dried droplet method. In this case, more sensitive lines shall be used, but they are generally not much broadened compared to the instrumental width, and more likely to be self-absorbed. Those two factors limit the accuracy of their Stark width measurement. In this work, the determination of the electron number density was indeed successful only for a few favorable metals, but remained within an estimated uncertainty of 2.5 10^{16} cm^{-3}. A common alternative would be to implement the Saha-Boltzmann method, but it is quite dependent on the uncertainty on the plasma temperature and the resulting uncertainty on the electron number density was not found better. Therefore, the dried droplet method, as implemented in this paper, was found limited to evidence a significant matrix effect on the electron number density.

Several comments can be made about the deposit itself. Regarding its composition, in principle any element that is not present in the samples can be used as a tracer element, provided it has favorable lines for spectroscopic diagnoses of the plasma. The concentration of the deposited solution can be easily adjusted so that the tracer lines are detectable without being self-absorbed. Also, the deposition method implemented in this work was very basic and can be improved in different ways to homogenize the residue and to increase the droplet wetting on the samples surface. For the dried droplet method to be valid, the presence of the residue on the sample surface should not modify the ablation efficiency, nor the plasma electron temperature and number density. Within our experimental uncertainties, we checked that those conditions were fulfilled using an iron chloride solution with a concentration up to 100 ppm, and a deposit on a 15x5 mm surface. However, more fundamentally, it might be possible that the iron atoms from the deposit are pushed by the expanding plasma and located in its periphery. Then, the plasma features as measured by this method would be more representative of this plasma region. As our experimental setup spatially integrated the plasma emission, it was not suited to investigate this point.

4. CONCLUSION

In this paper, the dried droplet method was successfully implemented to characterize matrix effects observed in LIBS analysis of metals with a 266 nm laser. This method consists in depositing a droplet of an iron-containing solution on the sample surface and ablating the dry residue. Then, iron lines are used for spectroscopic diagnoses of the plasma, and the ablated mass can be determined by white-light profilometry. Matrix effects mainly induce large differences in the number of ablated atoms, and much less pronounced differences in the plasma features, with more variation of the electron temperature compared to the electron number density. In further work, we will focus on the applicability of this approach to other types of samples, e.g. nonconductive ones, and on its exploitation for quantitative analysis of materials by LIBS.

5. AUTHOR STATEMENT

ER: Conceptualization, Methodology, Investigation, Formal analysis, Visualization, Writing; OM: Supervision, Writing – Reviewing and Editing; GL: Funding Acquisition, Writing – Reviewing and Editing; TV: Funding Acquisition, Project administration, Writing – Reviewing and Editing; JBS: Supervision, Project administration, Visualization, Writing.

6. DECLARATION OF COMPETING INTEREST

The authors declare that they have no known competing financial interests or personal relationships that could have appeared to influence the work reported in this paper.

7. ACKNOWLEDGEMENTS

The authors would like to thank Michel Tabarant for GD-OES analysis of the deposit. They also acknowledge financial support from CEA.

8. REFERENCES

[1] D. W. Hahn and N. Omenetto, “Laser-Induced Breakdown Spectroscopy (LIBS), Part II: Review of Instrumental and Methodological Approaches to Material Analysis and Applications to Different Fields,” *Appl. Spectrosc.*, vol. 66, no. 4, pp. 347–419, Apr. 2012, doi: 10.1366/11-06574.

[2] T. A. Labutin, A. M. Popov, V. N. Lednev, and N. B. Zorov, “Correlation between properties of a solid sample and laser-induced plasma parameters,” *Spectrochim. Acta Part B At. Spectrosc.*, vol. 64, no. 10, pp. 938–949, Oct. 2009, doi: 10.1016/j.sab.2009.07.033.

[3] L. M. Cabalín and J. J. Laserna, “Experimental determination of laser induced breakdown thresholds of metals under nanosecond Q-switched laser operation,” *Spectrochim. Acta Part B At. Spectrosc.*, vol. 53, no. 5, pp. 723–730, May 1998, doi: 10.1016/S0584-8547(98)00107-4.

[4] B. Sallé *et al.*, “Laser ablation efficiency of metal samples with UV laser nanosecond pulses,” *Appl. Surf. Sci.*, vol. 138–139, pp. 302–305, Jan. 1999, doi: 10.1016/S0169-4332(98)00495-4.

[5] S. Zhang, B. Zhang, W. Hang, and B. Huang, “Chemometrics and theoretical approaches for evaluation of matrix effect in laser ablation and ionization of metal samples,” *Spectrochim. Acta Part B At. Spectrosc.*, vol. 107, pp. 17–24, May 2015, doi: 10.1016/j.sab.2015.02.009.

[6] M. López-Claros, J. M. Vadillo, and J. J. Laserna, “Determination of plasma ignition threshold fluence during femtosecond single-shot laser ablation on metallic samples detected by optical emission spectroscopy,” *J. Anal. At. Spectrom.*, vol. 30, no. 8, pp. 1730–1735, 2015, doi: 10.1039/C5JA00076A.

[7] A. Ciucci, M. Corsi, V. Palleschi, S. Rastelli, A. Salvetti, and E. Tognoni, “New Procedure for Quantitative Elemental Analysis by Laser-Induced Plasma Spectroscopy,” *Appl. Spectrosc.*, vol. 53, no. 8, pp. 960–964, Aug. 1999.

[8] E. Grifoni, S. Legnaioli, G. Lorenzetti, S. Pagnotta, F. Poggialini, and V. Palleschi, “From Calibration-Free to Fundamental Parameters Analysis: A comparison of three recently proposed approaches,” *Spectrochim. Acta Part B At. Spectrosc.*, vol. 124, no. Supplement C, pp. 40–46, Oct. 2016, doi: 10.1016/j.sab.2016.08.022.

[9] J. Picard *et al.*, “Characterization of laser ablation of copper in the irradiance regime of laser-induced breakdown spectroscopy analysis,” *Spectrochim. Acta Part B At. Spectrosc.*, vol. 101, pp. 164–170, Nov. 2014, doi: 10.1016/j.sab.2014.08.029.

[10] E. A. Kaszewska, M. Sylwestrzak, J. Marczak, W. Skrzeczanowski, M. Iwanicka, E. Szmit-Naud, D. Anglos, and P. Targowski, “Depth-Resolved Multilayer Pigment Identification in Paintings: Combined Use of Laser-Induced Breakdown Spectroscopy (LIBS) and Optical Coherence Tomography (OCT),” *Appl. Spectrosc.*, vol. 67, no. 8, pp. 960-972, Aug. 2013.

[11] A.H. Galmed, A. du Plessis, S.G. le Roux, E. Hartnick, H. Von Bergmann, and M. Maaza, “Three dimensional characterization of laser ablation craters using high resolution X-ray computed tomography,” *Spectrochim. Acta Part B At. Spectrosc.*, vol. 139, pp. 75–82, Jan. 2018.

[12] D. W. Hahn and N. Omenetto, “Laser-Induced Breakdown Spectroscopy (LIBS), Part I: Review of Basic Diagnostics and Plasma–Particle Interactions: Still-Challenging Issues Within the Analytical Plasma Community,” *Appl. Spectrosc.*, vol. 64, no. 12, pp. 335–366, Dec. 2010, doi: 10.1366/000370210793561691.

[13] J. A. Aguilera, C. Aragón, V. Madurga, and J. Manrique, “Study of matrix effects in laser induced breakdown spectroscopy on metallic samples using plasma characterization by emission spectroscopy,” *Spectrochim. Acta Part B At. Spectrosc.*, vol. 64, no. 10, pp. 993–998, Oct. 2009, doi: 10.1016/j.sab.2009.07.007.

[14] A. M. EL Sherbini, A. M. Aboulfotouh, and C. G. Parigger, “Electron number density measurements using laser-induced breakdown spectroscopy of ionized nitrogen spectral lines,” *Spectrochim. Acta Part B At. Spectrosc.*, vol. 125, pp. 152–158, Nov. 2016, doi: 10.1016/j.sab.2016.10.003.

[15] Á. Villaseñor, C. Greatti, M. Boccongelli, and J. L. Todolí, “A dried droplet calibration approach for the analysis of solid samples through laser ablation – inductively coupled plasma mass spectrometry,” *J. Anal. At. Spectrom.*, vol. 32, no. 3, pp. 587–596, Mar. 2017, doi: 10.1039/C6JA00343E.

[16] Á. Villaseñor, M. Boccongelli, and J. L. Todolí, “Quantitative elemental analysis of polymers through laser ablation – inductively coupled plasma by using a dried droplet calibration approach, DDCA,” *J. Anal. At. Spectrom.*, vol. 33, no. 7, pp. 1173–1183, Jul. 2018, doi: 10.1039/C8JA00055G.

[17] C. Aragón and J. A. Aguilera, “Characterization of laser induced plasmas by optical emission spectroscopy: A review of experiments and methods,” *Spectrochim. Acta Part B At. Spectrosc.*, vol. 63, no. 9, pp. 893–916, Sep. 2008, doi: 10.1016/j.sab.2008.05.010.

[18] M. Ivković and N. Konjević, “Stark width and shift for electron number density diagnostics of low temperature plasma: Application to silicon Laser Induced Breakdown Spectroscopy,” *Spectrochim. Acta Part B At. Spectrosc.*, vol. 131, pp. 79–92, May 2017, doi: 10.1016/j.sab.2017.03.015.

[19] J. A. Aguilera, J. Bengoechea, and C. Aragón, “Curves of growth of spectral lines emitted by a laser-induced plasma: influence of the temporal evolution and spatial inhomogeneity of the plasma,” *Spectrochim. Acta Part B At. Spectrosc.*, vol. 58, no. 2, pp. 221–237, 2003.

[20] C. Chaléard, P. Mauchien, N. Andre, J. Uebbing, J. L. Lacour, and C. Geertsen, “Correction of Matrix Effects in Quantitative Elemental Analysis With Laser Ablation Optical Emission Spectrometry,” *J. Anal. At. Spectrom.*, vol. 12, no. 2, pp. 183–188, 1997, doi: 10.1039/A604456E.
[21] M. A. Ismail, H. Imam, A. Elhassan, W. T. Youniss, and M. A. Harith, “LIBS limit of detection and plasma parameters of some elements in two different metallic matrices,” *J. Anal. At. Spectrom.*, vol. 19, no. 4, pp. 489–494, 2004, doi: 10.1039/B315588A.